JOURNAL OF MATERIALS SCIENCE 25 (1990) 1392–1396

Crystallization and grain growth of melt-spun, amorphous $Cu_{60}Zr_{40}$

J. C. RAWERS, R. D. WILSON
United States Department of the Interior, Bureau of Mines, Albany Research Center, Albany, Oregon, USA

Crystallization and subsequent grain growth processes in melt spun ribbons of amorphous $Cu_{60}Zr_{40}$ ribbon were studied. The average grain size of samples was correlated with heat treating over the time interval 0.1 to 100 h and the temperature range 525 to 825° C using an Arrhenius type relationship. X-ray diffraction studies showed the principal phase formed by crystallization of amorphous $Cu_{60}Zr_{40}$ was $Cu_{10}Zr_7$. A two-stage, grain growth mechanism is proposed. The activation energy for the second stage of grain growth is 109 kJ mol^{-1}

1. Introduction

Since 1980, over 50 articles have been published on the mechanical and thermodynamic properties of rapidly solidified Cu–Zr alloys. Of these, approximately 40% are concerned with different aspects of crystallization. Crystallization of these alloys has been studied by differential scanning calorimetry (DSC) [1–5], by X-ray diffraction [6, 7], by ultrasonics [8], by high-resolution electron microscopy [3–5], and by Auger electron and Rutherford backscattering spectrometry [2]. Most of these studies have focused on experimental and theoretical [9] determination of grain nucleation activation energy. In a recent article, results from DSC combined with a new mathematical analysis technique were used to measure and determine the activation energy for both nucleation and growth of grains in amorphous CuZr metallic glass [9]. In the present study, melt-spun, amorphous ribbons were heat-treated, and the resulting crystal structure and the activation energy associated with the grain growth of the nonamorphous material were determined by measuring the grain area as a function of time and temperature.

This study is part of a programme to obtain thermodynamic and kinetic data related to the crystallization, nucleation, and grain growth of amorphous metals. Such data will be necessary if these materials are to be used for engineering applications.

2. Experimental procedures

Alloys with the nominal compositions shown in Table I were prepared by arc-melting 99.9% pure metals* on a water cooled copper plate under 0.1 atm argon. Four alloy compositions were prepared: (a) a slightly off-eutectic composition, $Cu_{60}Zr_{40}$, and three intermetallic compounds, (b) $Cu_{51}Zr_{41}$, (c) Cu_8Zr_3, and (d) $Cu_{10}Zr_7$. The intermetallic compositions were chosen because they represented the crystal phase structures into which the amorphous ribbon was expected to crystallize upon heat treating. After melting, the buttons were heat-treated at 900° C for 24 h. Chemical analysis of the alloys is presented in Table I.

The $Cu_{60}Zr_{40}$ was the only composition that was melt-spun. A general description of melt spinning and the melt-spin instruments has appeared elsewhere [10]. Melt spinning produced a ribbon approximately 10 mm wide and 0.01 mm thick.

X-ray data were obtained with Cu$K\alpha$ radiation by means of a conventional X-ray diffractometer. Diffraction patterns from the melt-spun ribbon were obtained from both sides of the ribbon. Diffraction patterns for the three intermetallic compounds were determined after the surfaces of the buttons had been machined flat and metallographically polished to a 600-grit finish.

To determine the grain growth characteristics of the melt-spun ribbon, samples were subsequently heat-treated in evacuated sealed quartz capsules that had been back-filled with a partial pressure of argon. Heat-treatment temperatures were 525, 575, 625, 675, 725, 775 and 825° C. Heat-treatment times were 0.1, 0.3, 1, 3, 10, 30 and 100 h (not all time–temperature combinations were used). To ensure that there was no oxidation of the ribbon during the heat treatments, zirconium powder was encapsulated with the ribbon. Part of each heat-treated sample was used for crystal phase studies using X-ray diffraction. The rest was saved for metallographic examination, image analysis, and grain growth determination.

Samples for grain growth studies were coated with epoxy, encapsulated in metallographic mounts, polished to a 0.1 μm finish, and then over-etched with Kroll's solution to help delineate the grain boundaries. Optical photographs were taken at 500 magnification (Fig. 1). Photographs were then enlarged, and the average grain size was determined by image analysis using a Kontrol image analysing system† (Table II). In most cases, several photographs were

*The Hf addition cited in Table I was also a pure metal powder. The Hf was added as part of a perturbed-angular-correlation (PAC) experiment. Because of the extreme chemical similarity between Hf and Zr, the total combined Hf and Zr concentration will be referred to as only Zr.

†Reference to specific products does not imply endorsement by the Bureau of Mines.

0022–2461/90 $03.00 + .12

TABLE I Alloy compositions (at %)

	Cu	Zr	Hf	O	Crystal structure (space group, space group number)
Melt spun eutectic	59.3 [60]*	38.7 [40]	1.9		
$Cu_{51}Zr_{14}$	78 [78.5]*	20 [21.5]*†	1.2	0.8	hexagonal (P6/m, 175)
Cu_8Zr_3	71 [72.7]*	25 [27.3]*†	2.2	1.1	orthorhombic (Pnma, 62)
$Cu_{10}Zr_7$	58 [58.8]*	39 [41.2]*†	2.5	0.8	orthorhombic (Aba2.41)

*Target composition.
†Target composition, Zr + Hf.

analysed for each heat treatment. The number of grains measured in each photograph varied from 37 to 183, the average being 132. Multivariant analysis was used for data reduction.

3. Data and analysis

X-ray diffraction patterns of the melt-spun ribbon showed the metal to be approximately 100% amorphous (Fig. 2a). After a heat treatment of 0.1 h the ribbons showed no sign of amorphous structure regardless of heat-treating temperature (Fig. 2b–e). X-ray patterns from the heat-treated ribbons were checked against X-ray patterns obtained from literature [9, 11–17] and against X-ray patterns obtained from the three previously mentioned arc-melted intermetallic compositions (Fig. 2). X-ray diffraction generally did not show the presence of ZrO_2 in either the arc-melted melt-spun or heat treated ribbon.

Theoretical calculations as well as experimental results showed extensive overlap between diffraction patterns of the different intermetallic phases with very few lines being unique to a particular crystal structure (Fig. 3). Therefore, to determine if $Cu_{10}Zr_7$ was present, the *D*-spacing 3.2985 corresponding to the (2 2 0) plane was used (Fig. 3a); for Cu_8Zr_3 the *D*-spacing 2.0385 corresponding to the (0 4 0) plane was used (Fig. 3b); and for $Cu_{51}Zr_{14}$ the *D*-spacing 2.2060 corresponding to the (2 2 3) plane was used (Fig. 3c). Each of the lines chosen had a relative intensity greater than 30% maximum line intensity in a powder pattern and had no interference peak with diffraction patterns from the other crystal structures.

From the Cu–Zr phase diagram [11], the lever rule predicts that at phase equilibrium the melt-spun composition should be approximately 93% $Cu_{10}Zr_7$. X-ray diffraction patterns of the short-time, heat-treated ribbons indicated primarily $Cu_{10}Zr_7$ (Fig. 2b). The diffraction pattern matched that of $Cu_{10}Zr_7$, however, intensities indicated moderate grain growth and some preferred orientation. At longer heat-treatment times, metallographic examination showed that the grain structure coarsened and the X-ray line intensities changed, indicating a more randomly oriented grain distribution characteristic of a powder diffraction pattern (Fig. 2c–f).

The onset of a much weaker second phase, Cu_8Zr_3 was observed at longer times at higher heat-treatment temperature, i.e. 1.0 h at 825° C (Fig. 2c). At 625° C, Cu_8Zr_3 was not observed until after 10 h of heat treatment (Fig. 2e). At 575° C, the Cu_8Zr_3 was not observed until after 100 h, and at 525° C it was not observed even after 100 h of heat treatment (Fig. 2f).

TABLE II Average grain size in recrystallized metal spun $Cu_{60}Zr_{40}$ ribbons

Temperature (° C)	Time (h)	Average grain size (10^{-8} m^2)	Standard deviation (10^{-8} m^2)	Number of photographs
525	3	1.22	0.20	3
	30	3.14	1.14	4
575	30	8.25	1.30	7
625	3	5.53	1.71	3
	30	14.06	2.64	3
675	30	40.2	4.28	1
725	3	30.12	2.17	2
	10	54.7	10.8	3
775	0.3	18.3	6.5	2
	3.0	47.22	11.8	2
825	0.1	24.82	7.30	1
	1.0	75.40	8.9	1

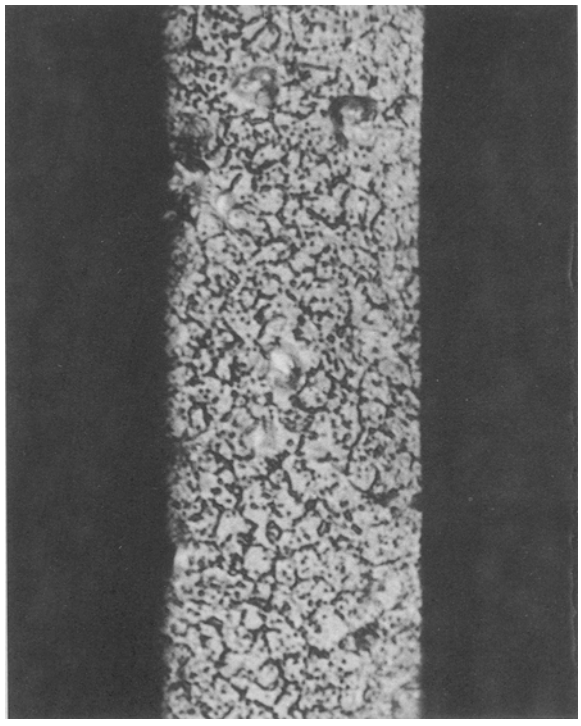

Figure 1 Cross section optical photographs of crystallized $Cu_{60}Zr_{40}$ ribbon. 625° C; 1.0 h; × 2500.

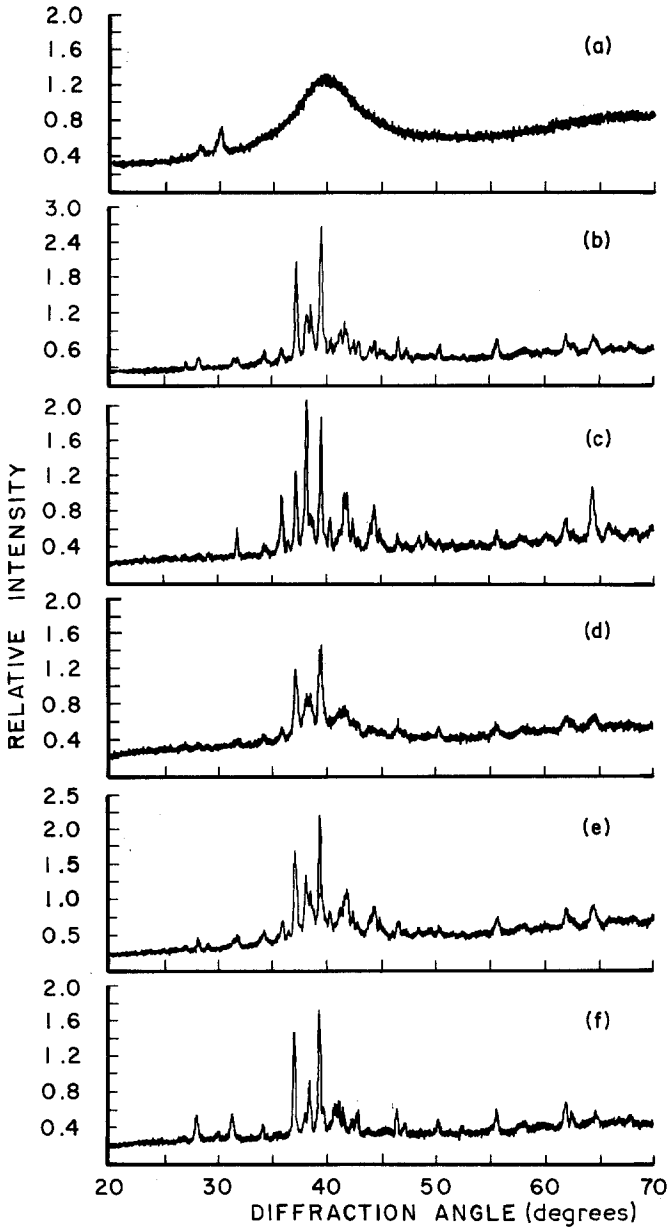

Figure 2 X-ray diffraction patterns of heat-treated melt-spun $Cu_{60}Zr_{40}$ ribbon. (a) Amorphous, melt-spun ribbon, (b) 825° C, 0.1 h, intensity pattern indicates preferred orientation, (c) 825° C, 100 h, similar intensity pattern to powder sample, (d) 725° C, 100 h, (e) 625° C, 100 h, (f) 525° C, 100 h, slight indication of $Cu_{51}Zr_{14}$.

The most recently published Cu–Zr phase diagram [11] indicates that Cu_8Zr_3 undergoes eutectoid decomposition on cooling below 612° C to form $Cu_{51}Zr_{14}$ and $Cu_{10}Zr_7$. To observe this decomposition, samples of the intermetallic button with composition Cu_8Zr_3 were heat treated at 550° C for 100 h. X-ray analysis showed the presence of both $Cu_{51}Zr_{14}$ and $Cu_{10}Zr_7$, indicating that the eutectoid transformation had occurred (Fig. 3d). However, heat treatment of the melt-spun $Cu_{60}Zr_{40}$ ribbon did not show the presence of the $Cu_{51}Zr_{14}$ phase for any of the heat treatments in this study (Fig. 2)

Grain growth was determined for the observed major phase, $Cu_{10}Zr_7$. Grain size (area) determinations are presented in Table II. The average grain size obtained from the image analysis was chosen as the representative value for each tature combination. The data were fitted to a modified Arrhenius equation,

$$\text{average grain size (in m}^2) = At^n \exp(-Q/RT) \quad (1)$$

where A is a constant, t is the time at temperature (h), n the time exponent, Q the activation energy for grain growth, R the gas constant and T the temperature (in K).

Statistical analyses of the fitted coefficients to Equation 1 are presented in Table III. The activation energy, Q, was determined to be $109(\pm 3)\,\text{kJ mol}^{-1}$ (Fig. 4), which is typical of grain growth controlled by bulk atomic diffusion. These results are in disagreement with previous studies by Wu *et al.* [9], who reported an activation energy of $411(\pm 25)\,\text{kJ mol}^{-1}$. The large difference in measured activation energies cannot be accounted for by experimental uncertainty. This difference can be explained, however, by hypothesizing that there are two stages of grain growth. During the initial heat treatment, the nucleated grains are in an amorphous metal matrix. The higher activation energy obtained by Wu *et al.* represents grain growth resulting from diffusion of atoms through the

TABLE III Fitted coefficients and statistical analysis for grain growth equation: average grain size $= At^n \exp(-Q/RT)$

	Coefficient	Standard error
Constant, A	16.2	0.50
Time exponent, n	0.42	0.035
Activation energy, Q (J mol^{-1})	109 700	3 920

Statistical fit: $R^2 = 0.98$.

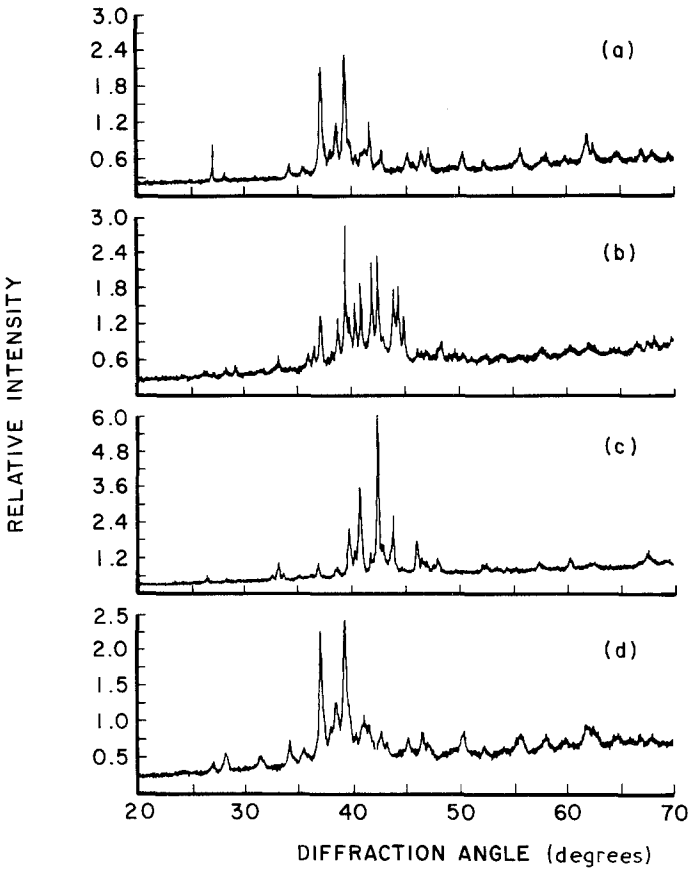

Figure 3 X-ray diffraction patterns of Cu–Zr intermetallics. (a) $Cu_{10}Zr_7$; (b) Cu_8Zr_3, quenched from 900° C; (c) Cu_8Zr_3, heat treated 100 h at 550° C; (d) $Cu_{51}Zr_{14}$.

amorphous matrix. Eventually the entire volume is composed of very small grains and the grains are in contact with one another, subsequent growth is now determined by bulk diffusion through a crystalline matrix and/or grain boundary migration. The lower activation energy measured in this study reflects this type of grain growth. That is, after the grains come into contact with one another, the grain growth requires a much lower activation energy and thus the rate of growth is drastically increased.

The time exponent, n, was determined to be 0.42. Grain growth exponents of 0.50 are predicted from most grain growth formulations based upon bulk diffusion theory. However, deviations of the time exponent from this value are routinely, experimentally obtained [18]. In fact, the time exponent is often found experimentally to be a strong function of temperature [19]. This was not observed for the temperatures used in this study (Fig. 4).

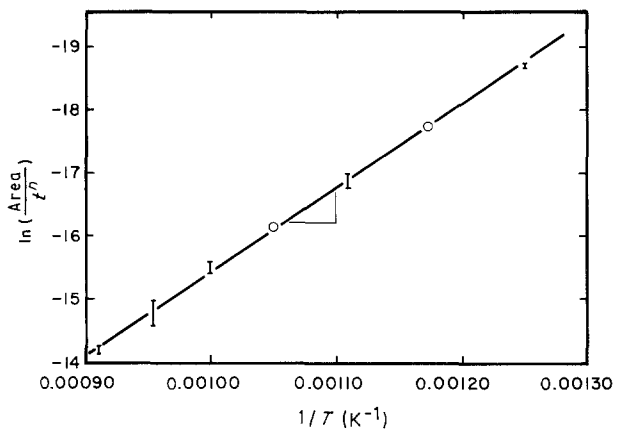

Figure 4 Determination of the apparent activation energy. Slope = Q/R, Q = 109 700 J mol^{-1}.

The consistent slope of the plot of grain diameter against time in Fig. 4 suggests that the data obtained from this experiment were consistent with the hypothesis that only one mechanism was responsible for grain growth. All the data were fitted to a linearized equation with an R^2 value of 0.98. The statistical variance in the grain size for each heat treatment accounts for most of the variance observed in the activation energy.

As the heat treatment progressed, a small, fine precipitate formed in the grain boundaries between the larger $Cu_{10}Zr_7$ grains and eventually formed a continuous phase surrounding each grain (Fig. 1). Although these precipitates coarsened with time, they were too small to accurately measure for grain growth. These grains were tentatively identified as Cu_8Zr_3. No attempt was made to determine the activation energy for growth of the second phase.

4. Conclusion

Crystallization of amorphous melt-spun $Cu_{60}Zr_{40}$ resulted in grain growth that consisted predominantly of $Cu_{10}Zr_7$. The activation energy for grain growth, experimentally determined by measuring the change in grain dimensions as a function of time and temperature, was 109 kJ mol^{-1}. This energy reflects the second stage of grain growth, after the amorphous matrix has been crystallized. At higher temperatures, X-ray diffraction showed the presence of a second phase, tentatively identified as Cu_8Zr_3. At temperatures below 575° C, the only phase observed, even after 100 h at temperature, was $Cu_{10}Zr_7$.

References

1. J. JANSSON and M. NUGREN, *J. Less-Common Metals* **1–2** (128) (1967) 319.

2. E. C. STELTER, *Diss. Abstr. Int.* **46** (7) (1986) 171.
3. M. A. OTOONI, "Rapidly Solidified Metastable Materials" (Elsevier, New York, 1983).
4. *Idem*, Conference Electron Microscopy, Materials Science, Hamburg, West Germany, August 17–24, 1982.
5. *Idem*, Conference Alloy Phase Diagrams, Boston, MA, November 1982.
6. K. DINI and R. A. DUNLAP, *J. Phys. F. Met. Phys.* **15** (2) (1985) 273.
7. G. A. STERGIOUDIS, J. GASTALDT and C. JOURDAN, *Mater. Res. Bull.* **20** (3) (1985).
8. J. C. CHANG, F. NADEAU, M. ROSEN and R. MEHRABIAN, *Scripta Metall.* **16** (9) (1982) 1073.
9. Q. C. WU, M. HASRMELIN, J. BIGOT and G. MARTIN, *J. Mater. Sci.* **21** (10) (1986) 3581.
10. M. SMITH and M. SALATORE, *Rev. Sci. Instr.* **57** (8) (1986) 1647.
11. E. KNELLER, Y. KHAN and U. GORRES, *Z. Metallkde* **77** (1) (1986) 43.
12. J. P. GABATHULER, P. WHITE and E. PARTHE, *Acta Cryst.* **15** (1975) 894.
13. L. BSENKO, *ibid.* **B-32** (1976) 2220.
14. M. E. KIRKPATRICK, J. F. SMITH and W. L. LARSEN, *ibid.* **15** (1962) 894.
15. L. BSENKO, *J. Less-Common Metals* **40** (1975) 365.
16. J. L. GLIMOIS, P. FOREY, J. FERON and J. BECLE, *ibid.* **78** (1981) 45.
17. E. M. CARVALHO and I. R. HARRIS, *J. Mater. Sci.* **15** (1980) 1244.
18. R. E. REED-HILL, "Physical Metallurgy Principles", 2nd ed. (D. van Nostrand Co., New York) p. 309.
19. R. L. FULLMAN, ASM Seminar, Metal Interfaces (1952) p. 179.

Received 22 November 1988
and accepted 8 May 1989